Microphysical Structure of the Marine Boundary Layer under Strong Wind and Spray Formation as Seen from Simulations Using a 2D Explicit Microphysical Model. Part I: The Impact of Large Eddies

J. SHPUND, M. PINSKY, AND A. KHAIN

Department of Atmospheric Sciences, The Hebrew University of Jerusalem, Jerusalem, Israel

(Manuscript received 25 August 2010, in final form 23 May 2011)

ABSTRACT

The effects of large eddies (LE) on the marine boundary layer (MBL) microphysics and thermodynamics is investigated using a 2D Lagrangian model with spectral bin microphysics including effects of sea spray. The 600 m × 400 m MBL computational area is covered by 3750 adjacent interacting Lagrangian parcels moving in a turbulent-like flow. A turbulent-like velocity field is designed as a sum of a high number of harmonics with random time-dependent amplitudes and different wavelengths including large eddies with scales of several hundred meters. The model explicitly calculates diffusion growth/evaporation, collisions, and sedimentation of droplets forming both as sea spray droplets and background aerosols, as well as aerosol masses within droplets. The turbulent mixing between parcels is explicitly taken into account. Sea spray generation is determined by a source function depending on the background wind speed assumed in the simulations to be equal to 20 m s^{-1}. The results of simulations obtained by taking into account the effects of LE are compared to those obtained under the assumption that the vertical transport of droplets and passive scalars is caused by small-scale turbulent diffusion. Small-scale turbulence diffusion taken alone leads to an unrealistic MBL structure. Nonlocal mixing of the MBL caused by LE leads to the formation of a well-mixed MBL with a vertical structure close to the observed one. LE lead to an increase in the sensible and latent heat surface fluxes by 50%–100% and transport a significant amount of large spray droplets upward. Microphysical processes lead to formation of spray-induced drizzling clouds with cloud base near the 200-m level.

1. Introduction

A new wave of interest in detailed descriptions of ocean–atmosphere interaction in areas associated with strong winds was triggered by the results obtained by Powell et al. (2003), who analyzed hurricane boundary layer (BL) wind profiles measured using Global Positioning System (GPS) sondes. The potential temperature and specific humidity soundings indicated the presence of a well-mixed boundary layer with mean wind profiles close to logarithmic. The observed changes in the vertical profiles of wind speed occurring with increasing wind speeds were attributed to a decrease in the surface roughness and the drag coefficient for wind speeds exceeding about 33 m s^{-1}. This decrease was attributed to the development of a sea foam layer at the air–sea interface. It was suggested that foam coverage could progressively form a ''slip'' surface at the air–sea interface. In addition, Powell et al. (2003) suggested that sea spray significantly influences the transfer of momentum, heat, and moisture and proposed an alternative scenario to explain the observed wind profiles. This explanation is related to the existence of linear coherent features in the form of helical rolls [large eddies (LE)] in the boundary layer. Powell et al. (2003) hypothesized that at low levels GPS sondes could be preferentially drawn into a convergent and downward part of a helical roll circulation that would contain the strongest winds, contributing to a profile with smaller shear (lower friction velocity) near the surface. Several studies elaborate this hypothesis.

The effect of LE on the structure of the marine boundary layer (MBL) under strong winds was investigated by Ginis et al. (2004) in more detail. The existence of such eddies with characteristic scales of several hundred meters (often identified as convective cells) in both unstable and neutral MBLs is well known (e.g., LeMone

Corresponding author address: Prof. Alexander Khain, Department of the Atmospheric Sciences, The Hebrew University of Jerusalem, Jerusalem, Israel.
E-mail: khain@vms.huji.ac.il

DOI: 10.1175/2011JAS3652.1

1973; Ivanov and Khain 1975, 1976a; Stevens et al. 1999). Foster (2005), Lorsolo et al. (2008), and Zhang et al. (2008) reported that LE are an inherent phenomenon of a TC boundary layer. Ginis et al. (2004) showed that strong winds typical of a hurricane BL trigger formation of vortices (rolls) within the BL, where they are directed along the background wind direction. These vortices are easily identified by ''cloud streets'' forming in the areas of updrafts. Khain et al. (1986), Khain and Ingel (1988, 1995), and Ginis et al. (2004) showed that these vortices transport high momentum down from upper levels to the surface level, thereby increasing the surface wind speed. In case of strong winds at the top of the BL, the increase in surface wind can reach about 10–12 m s^{-1} (Ginis et al. 2004). Furthermore, these vortices transport humidity from the surface layer aloft, increasing the humidity gradient in the surface layer, which in turn leads to an increase in the latent heat surface flux. Large eddies were found to affect surface sensible heat flux as well.

Another line of studies attributes the increase in surface wind speed to sea spray forming in regions of strong winds. The main mechanism discussed in these studies is the direct effect of sea spray (i.e., heavy particles) on the vertical stratification of density that affects buoyancy and weakens the turbulent mixing. Suppression of turbulent mixing in the lower part of the boundary layer should lead to airflow acceleration and reduction of the surface drag (e.g., Toba 1965; Davidson and Schutz 1983; Fairall et al. 1990, 1994; Powell et al. 2003; Makin 2005; Kudryavtsev 2006). Ingel (2011), who investigated this mechanism in detail by solving a nonlinear equation system for turbulent kinetic energy, dissipation energy, and turbulent viscosity, found that sea spray mass produced in a tropical cyclone (TC) BL is not large enough to significantly weaken the surface layer turbulence (and thus the drag coefficient) as would be required to explain observations of Powell et al. (2003).

The role of sea spray is not restricted to the surface layer dynamics in the vicinity of the ocean surface. There are several mechanisms by means of which sea spray can potentially affect surface sensible and latent fluxes as well as temperature and humidity of the entire maritime BL. On the one hand, formation of sea spray increases the effective evaporative surface. On the other hand, spray evaporation ceases under high relative environmental humidity. Moreover, high salinity allows spray droplets to grow under subsaturated conditions, which in turns decreases environmental humidity. Sea spray is known to be the main source of giant cloud condensational nuclei (GCCN) over oceanic regions, which affects cloud microphysics and rain formation (e.g., Rosenfeld et al. 2002; Andreae and Rosenfeld 2008). Sea spray has potential thermodynamic and microphysical effects on the atmospheric BL because of its functioning as drops and GCCN. To evaluate all these variety of effects, it is important to adequately describe the vertical distribution of spray mass as well as spray droplet size distributions at different levels, including those close to cloud base.

Investigating the variety of possible spray effects requires quite complicated models rich both in dynamics and in microphysics. There are two main types of models used to investigate spray dispersion and the corresponding thermodynamic effect. The first type includes Lagrangian models where trajectories of a large amount of spray droplets within the surface layer are simulated by solving the Langevin equation, which mimics the process of turbulent diffusion in the vicinity of a wavy ocean surface (Andreas 1995; Edson et al. 1996; Mestayer et al. 1996; Edson and Fairall 1994; Van Eijk et al. 2001). This approach was further elaborated by Mueller and Veron (2009), who applied a more realistic wavy surface representation. In addition, the correlation function characterizing the particle motion in a turbulent flow was extended to the anisotropic nonstationary case. Averaging over spray droplet trajectories allows one to determine a vertical profile of the droplet-mediated humidity flux. These models have several disadvantages: they are applicable only within a limited height not exceeding several meters and they do not enable proper evaluation of changes in air temperature and humidity, caused by droplet growth/evaporation, or of the consequent impact of these changes on droplet spectra and aerosol spectra.

The second type of models includes 1D Eulerian models in which turbulent diffusion of sea spray away from the ocean surface source is assumed to be compensated by the gravitational sedimentation of spray droplets. This assumption leads to a power-law decay of spray concentration with height and allows one to express the vertical gradient of spray loading through the droplet fall velocity, as well as to evaluate the decrease in the production of turbulent kinetic energy within the surface layer, caused by spray formation (e.g., Rouault et al. 1991; Edson and Fairall 1994; Makin 1998; Fairall et al. 2009; Ingel 2011). While describing spray droplet dispersion, most of these 1D models impose upper boundary conditions on heights on the order of tens of meters and do not address the effects of droplet salinity (e.g., Rouault et al. 1991; Edson and Fairall 1994; Makin 1998).

The model developed by Kepert et al. (1999) (with later improvements) can be considered as the most advanced 1D Eulerian model that treats sea spray droplets. The variables are calculated at 36 logarithmically spaced

height levels at the surface and blend smoothly into a linear spacing near the upper boundary at 6.5 km. The 1.5-K theory closure scheme is applied to calculate the effects of spray loading on turbulent kinetic energy. In addition, the model (a) applies the equation for diffusion growth/evaporation of spray drops that takes into account spray salinity, (b) calculates spray droplet concentration as a function of height as well as of droplet radius, and (c) uses the equations for turbulent diffusion and evaporation to determine spray droplet fluxes, as well as the changes of spray size caused by evaporation. This model is the basis of the currently used spray parameterization module in operational TC models (e.g., Bao et al. 2007, 2009).

Despite the significant achievements in description of sea spray effects, many problems concerning spray transport and thermodynamic interactions are still not well understood. This can be partly accounted for by the limitations of the models currently in use. The models that are rich in dynamics (e.g., Stevens et al. 1999; Ginis et al. 2004; Xue and Feingold 2006) do not include sea spray treatment. At the same time, most of the 1D models that treat sea spray dispersion are actually surface layer models, where the vertical transport of spray is associated with turbulent diffusion only. The small-scale turbulent diffusion is described using the local 1.5-K theory closure scheme (e.g., Kepert et al. 1999). Being local, this closure scheme describes the effects of turbulent vortices with scales much less than the depth of the surface layer. At the same time, the effects of large eddies on the scale of several hundred meters (i.e., scales of BL depth) are not taken into account. It should be noted that updrafts in LE (i.e., convective cells) having time scales of about 10 min can easily reach 1–4 m s^{-1}, which exceeds fall velocities of most spray droplets (e.g., Ginis et al. 2004; Zhang et al. 2008, 2009; Zhang 2010, and references within). The vertical transport within the BL is largely determined by LE (e.g., Stull 1988; Garratt 1994; Ginis et al. 2004), thus making LE a quite important factor in vertical distribution of spray droplets.

The sea spray microphysics that is currently in use in 1D spray models is simplified compared to that used in advanced microphysical cloud models. Utilization of the 1D geometry does not allow accurate calculation of the droplets' vertical transport. Furthermore, the 1D model configuration is problematic for calculating supersaturation (or subsaturation), which in turn determines the diffusion growth/evaporation rate (Stevens et al. 1998). It is known that supersaturation values as well as rates of diffusion growth/evaporation in the BL crucially depend on the sign and the magnitude of the vertical updrafts in the BL (e.g., Magaritz et al. 2009). These effects can hardly be accurately represented within the frame of a 1D model where the mean vertical velocity is assumed to be equal to zero (e.g., Kepert et al. 1999).

Another drawback of current spray models is not taking into account the maritime "background" aerosol particles (APs) that always exist over the open ocean. The concentration of these APs is on the order of about 200 cm^{-3} (e.g., Stevens et al. 2003, 2005), with most of these APs being soluble and of wet size (i.e., haze size) that may exceed a few microns in radius. The concentration of background APs at moderate wind speed is higher than that of spray droplets by at least one order of magnitude. The APs give rise to cloud formation everywhere over the oceans, and their effects on spray evolution may be significant, especially in areas of spray source location. We hypothesize that a pronounced interaction of spray with background aerosols takes place also in areas of cloud formation. Spray growth by diffusion (condensation) and possibly by collisions should allow spray droplets to grow beyond their initial radius; however, the model suggested by Kepert et al. (1999) does not allow spray droplets to grow beyond their initial radius.

These simplifications limiting the applicability of the models described above call for an improvement regarding treatment of the dynamical and microphysical processes in order to understand the role of spray with regard to the thermodynamic and microphysical structure of the MBL at strong winds. In the present study, we investigate the effects of LE under sea spray production conditions by means of a 2D BL spectral microphysical model (Khain et al. 2008; Pinsky et al. 2008; Magaritz et al. 2009). This model has been successfully used for simulations of the microphysical and thermodynamic structure of the cloud-topped BL as well as for simulation of droplet size distribution (DSD) and drizzle formation in stratocumulus clouds. For the purposes of the present study, the model has been updated to take into account the production and transport of various spray droplets by vortices of different scales including large eddies, as well as an explicit saline droplet bin microphysics module. The major objectives of the following studies include 1) evaluating the role of large vortices role in vertical distribution of sea spray and the effects of large eddies on surface fluxes, 2) evaluating sea spray microphysical effects on MBL thermodynamics as well as sensible surface fluxes and latent heat surface fluxes, 3) evaluating the impact of different microphysical processes (diffusion growth, sedimentation, and collisions) and the impact of the background maritime aerosols on temperature and humidity across the MBL, and 4) describing spray size distributions at different heights.

It is impossible to address all these problems within the frame of one paper. In this study we mainly address

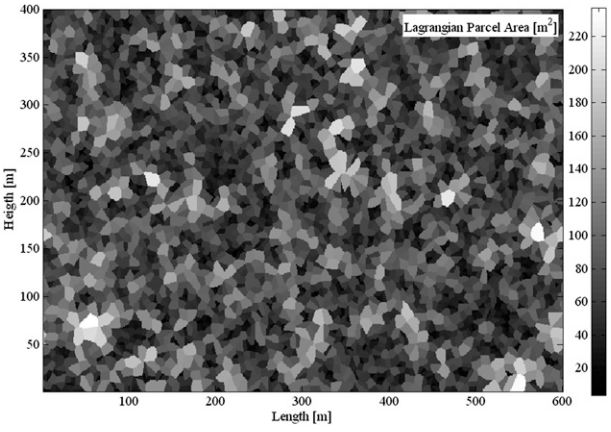

FIG. 1. The model computational area as seen from the parcel area field. The Lagrangian parcels move within a turbulent-like flow containing a wide range of harmonics including large eddies. The computational area is 600 m (horizontally) × 400 m (vertically) and is covered with 3750 adjacent Lagrangian air parcels with a characteristic linear size of ~8 m.

the first problem, namely the effect of LE on the structure and microphysics of MBL under sea spray production conditions.

2. Model description and simulation design

a. The model

Since the model is described in detail by Pinsky et al. (2008) and Magaritz et al. (2009), we present here only a brief description. The latest improvements related to turbulent mixing between parcels, surface flux calculation, and sea spray formation are described in more detail. The computational area 600 m long × 400 m high is covered by 3750 interacting adjacent Lagrangian air parcels with a characteristic linear size of about 8 m (Fig. 1). These parcels move within a turbulent-like velocity field generated by a turbulent flow model. This field is represented as a sum of a large number of harmonics with random time-dependent amplitudes and is assumed to be statistically uniform horizontally. The velocity field obeys the turbulent laws at high wavenumber (e.g., the Kolmogorov $-5/3$ law) in agreement with observed data (Zhang et al. 2009). The model parameters are calculated to agree with the correlation properties of the velocity field. Harmonics of the largest wavelengths play the role of large eddies with scales of several hundred meters and a lifetime of several minutes.

At the initial time instance, the Lagrangian air parcels are assumed to be equal and are distributed uniformly over the entire area. The parcels transport potential temperature and mixing ratio as well as aerosols and droplets. In the new version of the model, the parcels also transport sea spray droplets. Microphysics of each Lagrangian cloud parcel include the diffusion growth/evaporation equation used for wetted aerosols and water droplets, as well as the equation for supersaturation and the stochastic collision equation describing collisions between droplets (Pinsky and Khain 2002; Pinsky et al. 2008). The DSD of both the nonactivated APs and the cloud droplets is calculated on a mass grid containing 500 bins within the 0.01- to 1000-μm radius range. The mass of each bin in each parcel changes with time according to the equation for diffusion growth. A short time step (0.01 s) is used to adequately simulate the growth of the smallest APs, so the size separation between the nonactivated nuclei attaining equilibrium with environment (i.e., haze particles) and the growing droplets is simulated explicitly, without any parameterization of droplet nucleation. Droplet collision growth is calculated by solving the stochastic collision equation; collision kernels and collision efficiencies between droplets of different size were taken from tables calculated by Pinsky et al. (2001) with a high 1-μm resolution in droplet radii. Collisions are calculated using a 1-s time interval.

The model calculates the AP budget treating APs in two ''states'': nonactivated wet APs (haze particles) and APs dissolved within droplets. The mass of APs (i.e., mass of salt) in droplets does not change in the course of the condensation/evaporation process, while in case of collision/coalescence the dissolved AP mass in the drop collectors increases. The total droplet evaporation leads to formation of wet APs. A specific feature of spray particles is their high salinity, which affects their thermodynamic behavior. Throughout droplet collisions, the AP size distribution changes during the parcel motion within the BL. At $t = 0$, the BL is cloud-free, and all the parcels contain only nonactivated APs. In the ascending parcels, nonactivated aerosols and droplets can exist simultaneously. If supersaturation in a parcel is replaced by subsaturation, droplets may evaporate partially or totally. In the latter case, the cloud parcel contains only nonactivated wet aerosols. The process of droplet settling is taken into account explicitly. The algorithm for settling represents an extension of the well-known flux method (e.g., Bryan 1966; Bott 1989) describing the advection and particle sedimentation in the Eulerian models with irregular finite difference grids to irregular grids formed by the centers of the parcels. In this sense, the model can be referred to as a hybrid Lagrangian–Eulerian model.

In the model, the effects of the microphysics on the dynamic (turbulent) structure are not taken into account explicitly. Instead, we generate a turbulent-like structure

using the basic statistical parameters of the flow taken from observations. The most important parameter is the rms of vertical velocity fluctuations profile, namely $\sigma_w(z) = \langle w'^2 \rangle^{1/2}$, where w' are the fluctuations of vertical wind velocity and the angle brackets symbolize horizontal averaging. In nature, the BL dynamical structure is formed under the combined effects of many factors such as latent heat release, thermal instability, wind shear, and surface heat and moisture fluxes. In assimilating the real dynamics, we implicitly take into account all these factors.

The model takes into account the turbulent mixing between Lagrangian parcels following the study conducted by Pinsky et al. (2010a). The mixing represents an extension of the classical K theory (1.5-order closure) to the case of mixing of nonconservative values such as size distributions. The rate of mixing depends on the distance between the parcel centers. The turbulent diffusivity coefficient is calculated using the Richardson 4/3 law. The turbulent mixing between the parcels takes place when the separation distance between their centers is below about 30 m; this value is considered as the typical mixing length in the BL. The heat and moisture surface fluxes are calculated in the model using the standard bulk aerodynamic formulas. The air–sea temperature and humidity gradients are calculated as differences between the corresponding values at the ocean surface and at the centers of the parcels at 10-m level.

Since roll vortices (large eddies) tend to be directed along the background wind, the model computational area (Fig. 1) is interpreted in this study as a cross section perpendicular to the background hurricane wind.

b. Spray treatment and the background aerosol

The dominant mechanisms for sea spray production are the burst of the rising air bubbles that are injected below the sea surface by breaking waves, and the tearing of droplets from wave crests (Lewis and Schwartz 2004). The rate of spray production and droplet size distribution are known to be associated primarily with increasing wind speeds. Recent studies have shown that the size range of sea spray droplets could be as wide as about 0.01 to about 500 μm (Mårtensson et al. 2003; Gong 2003; Clarke et al. 2006; Fairall et al. 2009). Typically, in sea spray dispersion models, only spray droplets that exceed about 10 μm in radius are considered. These drops determine the vertical loading gradient. From the microphysical point of view, however, droplets of smaller sizes may also play a role since they can ascend to high levels and contribute significantly to the budget of GCCN and spray droplets, affecting cloud microphysics and warm rain formation. In this study, a wind-dependent source function describing the production rate of spray droplets of different sizes per area unit per time unit was constructed by matching two size-resolved sea spray source functions for both the small and the large droplet sizes. The ultramicron regime (i.e., ''spume'' droplets with radii ranging from 10 to about 500 μm) was reproduced after the parameterization used by Fairall et al. (2009), while the submicron regime (i.e., ''jet'' droplets with radii ranging from about 0.01 to about 10 μm) was reproduced after Monahan et al. (1986), Mårtensson et al. (2003), Gong (2003), and Clarke et al. (2006) [see review by O'Dowd and de Leeuw (2007)]. The various submicron source function parameterizations were recalculated for 98% relative humidity (corresponding to water vapor equilibrium above ocean water with typical salinity of 35 g kg^{-1}) and then averaged to produce an average submicron spray source function. Figure 2a presents the spray source parameterizations renormalized for 98% RH, along with the averaged submicron source function, the well-known Andreas (1998) source function, and an example of the matched source functions (all of the above for wind speed $U_{10} = 30$ m s^{-1}). The matching point between the source functions of ultra- and submicron droplets is around 10-μm droplet radius and slightly wind speed dependent. The source functions calculated for the background wind speed of 20 m s^{-1} used in the present study are shown in Fig. 2b. The location of the maximum of the source function over the mean surface level was assumed to be wind speed-dependent (C. Fairall 2010, personal communication). The vertical profile of the source function was assumed to be of a triangle shape as $S(z) = S_o(1 - 2|z - H_{\text{wave}}|/H_p)$, where H_{wave} is the wave height calculated as $H_{\text{wave}} = 1 + 0.25V_{10}$ (C. Fairall 2010, personal communication), V_{10} is the background wind speed at 10-m height, and H_p is a parameter chosen to be equal to the parcel size (i.e., ~8 m).

In this study, the distribution of aerosol measured over the ocean during the Second Dynamics and Chemistry of Marine Stratocumulus field study (DYCOMS II) at winds below 10 m s^{-1} was chosen as the background (initial) distribution of dry APs (Magaritz et al. 2009) (Fig. 3). The concentration of background APs with dry radii below 1.3 μm is about 200 cm^{-3}, which significantly exceeds the concentration of spray within the corresponding radius interval for moderate wind speeds (approximately less than 10 m s^{-1}). The increase in concentration of small APs at stronger winds is taken into account by the source function (Fig. 2).

At $t = 0$, only background APs at subsaturation conditions are allowed. These APs begin growing toward the size ensuring equilibrium with the environment. At $t > 0$, the spray source with initial salinity equal to that of ocean water is switched on. The spray source function

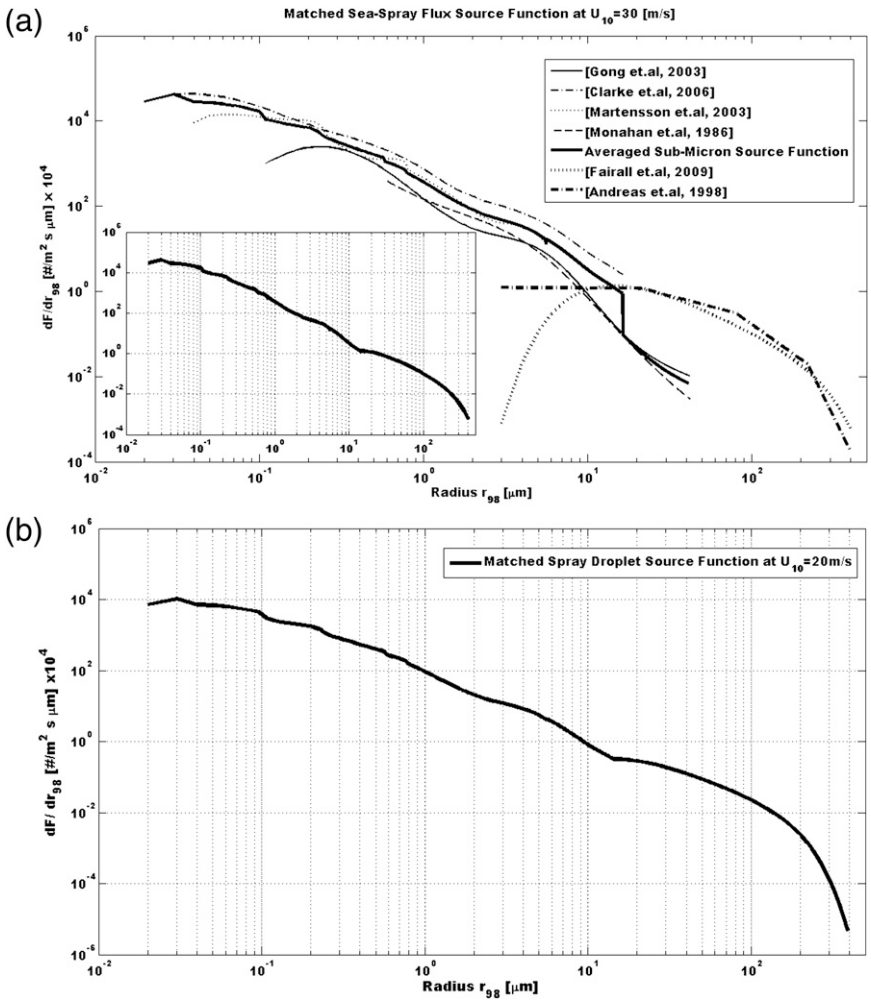

FIG. 2. (a) Matched size distribution of spray droplet source functions at $U_{10} = 30$ m s^{-1}. The submicron/micron source function distributions (i.e., jet droplets) were reproduced after their indicated original papers. The ultramicron source function distribution (i.e., spume droplets) was reproduced after the Fairall et al. (2009) parameterization. The inlay is the matched spray droplet source distribution. (b) Matched size distribution of spray droplet source function at $U_{10} = 20$ m s^{-1}, used in the No_LE and LE simulations.

used during the model integration changes the size distributions in the Lagrangian parcels adjacent to the ocean surface.

c. Simulation design

The amplitudes of velocity harmonics (including the intensity of large eddies) are calculated using the vertical profile of $\sigma_w = \langle w'^2 \rangle^{1/2}$ as described in detail by Pinsky et al. (2008). This profile typically shows a maximum in the middle of the BL (~200–400 m) and tends to vanish both at the surface and at the upper boundary of the BL, which is associated with the level of inversion (Lenschow et al. 1980; Lothon et al. 2005; Van Zanten et al. 2005; Pinsky et al. 2010b). In this study, the background wind was chosen to be equal to 20 m s^{-1} (the spray source function corresponding to this wind speed is shown in Fig. 2b). The friction velocity u_* corresponding to this wind speed is about 0.9–1 m s^{-1} (French et al. 2007). Analysis of tropical cyclone BL measurements (Zhang et al. 2009) shows that $\sigma_w/u_* \approx 1.25 \pm 0.25$ without any pronounced changes over height. Accordingly, in the present study $\langle w'^2 \rangle^{1/2} = 1.22\,\mathrm{m\,s^{-1}}$ was chosen. Typically, the $\langle w'^2 \rangle^{1/2}$ profile vanishes at the inversion level. At the same time, Zhang et al. (2009) did not find such vanishing of $\langle w'^2 \rangle^{1/2}$ at the inversion level in the BL of TCs. Despite this result, we used the condition $\langle w'^2 \rangle^{1/2}$ at the upper boundary of the computational area. The vertical profile of $\langle w'^2 \rangle^{1/2}$

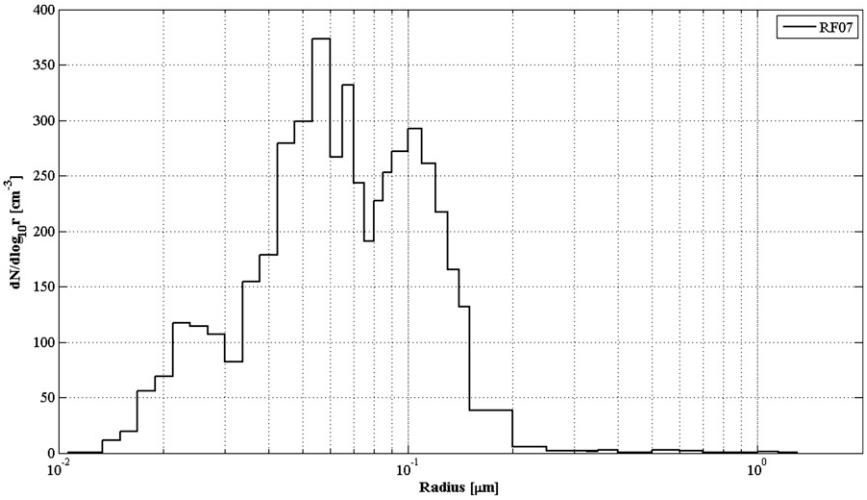

FIG. 3. Size distribution of dry aerosols in research flight RF07 during DYCOMS II, used in simulation as background aerosols.

used for the generation of velocity field is shown in Fig. 4. Our choice of the upper boundary height was influenced by the necessity of isolating the effects of large eddies in the MBL in the presence of spray. Using a computational area of a larger height would make it necessary to consider formation of cumulus clouds, which is beyond the scope of the present paper and will be the focus of a separate study. The assumption of $\langle w'^2 \rangle^{1/2} = 0$ at the upper boundary is likely to underestimate the calculations of large eddies' effects over vertical spray transport at high levels. However, we believe that the choice of the upper boundary at 400 m allows us to investigate the role of large eddies, at least qualitatively. Note that according to measurements taken at the Coupled Boundary Layers Air–Sea Transfer (CBLAST) experiment in the outer rainbands, Zhang et al. (2009) suggested a schematic conceptual model that implies the height of the mixing layer to be around 400 m (Zhang et al. 2009; see their Fig. 10). The well-known expression for the dissipation rate $\varepsilon = CE^{3/2}/l$ was used, where E is the turbulent kinetic energy, l is the mixing length assumed to be equal to 30 m, and $C = 0.2$; the dissipation rate is evaluated as 0.025 $m^2\ s^{-3}$, which agrees well with observations (Zhang et al. 2009; Zhang 2010). Figure 5 shows power spectra of vertical velocity w'^2 calculated at the height of 200 m and horizontal velocity v'^2 calculated at the height of 30 m where horizontal fluctuation component is most significant. One can see that both

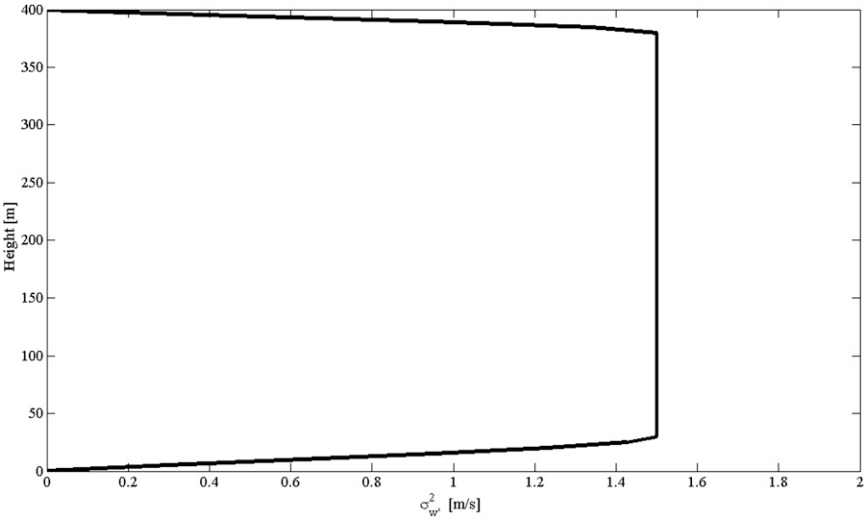

FIG. 4. Horizontally averaged $\sigma_w^2 = \langle w'^2 \rangle(z)$.

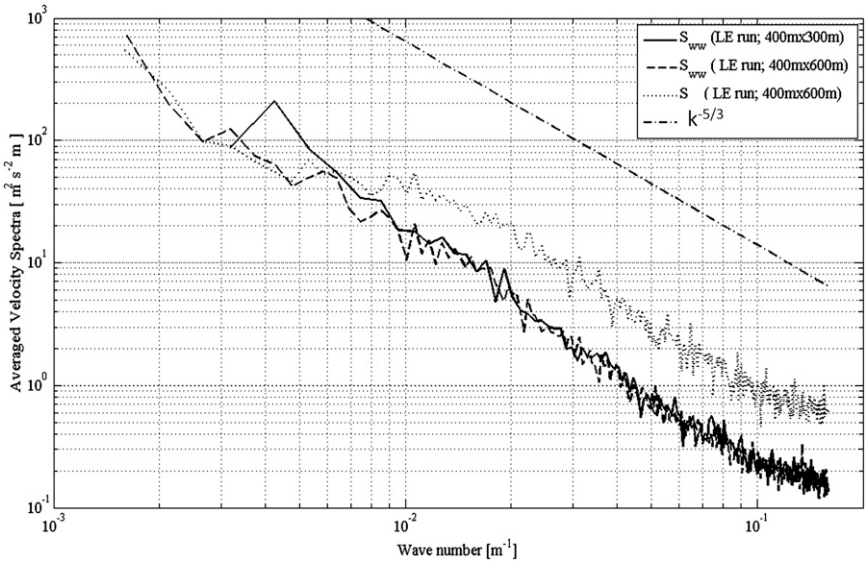

FIG. 5. Wind speed averaged spectra corresponding to vertical and horizontal turbulence of the given dependence $\sigma_w^2 = \langle w'^2 \rangle(z)$. Vertical spectra of the 400 m × 300 m (solid) and 400 m × 600 m (dashed) LE runs shows maximum eddy horizontal lengths (per wavenumber) of about 300 and 600 m, respectively. The Kolmogorov $-5/3$ slope is shown as a dashed–dotted line.

components obey the Kolmogorov $-5/3$ law in agreement with observations. Sensible surface fluxes and latent heat surface fluxes were calculated using bulk-aerodynamic formulas with a Dalton number of $C_E = 0.001\ 18$ (Drennan et al. 2007).

To investigate the role of large eddies transporting air parcels over the entire computational area, the results of the two primary (control) simulations were compared. In the first simulation, all dynamical and microphysical processes were taken into account. This run includes large eddies and will be referred to hereafter as the LE run. The second run is similar to the first run with one important exception, namely that the maximum of the $\langle w'^2 \rangle^{1/2}$ profile was set to be equal to 0.001 m s^{-1}. In this case, advection of air parcels by the ''mean'' velocity was excluded. Therefore, in this simulation the upward transport of scalar variables and droplet size distribution, including spray droplets, is determined by the turbulent mixing between the air parcels (i.e., by turbulent diffusion only). The second run will be referred to as the No_LE run (i.e., it has no large eddies). The dynamic conditions of this run are similar to those used in 1D Eulerian models of the surface/boundary layers.

It should be noted that velocity fields generated by turbulent-like model represent a random realization of turbulent velocity. To justify the robustness of the results, they should be close in different turbulent velocity field statistical realizations. Another question to be answered concerns the sensitivity of the results to the choice of the horizontal size of the computational area. It is known that the aspect ratio (the ratio of the horizontal size of the convective cell to the vertical size) in the atmospheric BL varies within a wide range from about 1.5 to 10 (e.g., Ivanov and Khain 1976b). The reason for such variability is not well understood. To justify the stability of the results with respect to different realizations of turbulent velocity, as well as to the choice of the horizontal size of the computational area, two supplementary simulations were performed, one with a computational area 600 m long and the other 300 m long, and both with velocity realizations different from those used in the control runs.

The initial profiles of potential temperature and mixing ratio were taken as in Kepert et al. (1999) (and are shown in our Figs. 9 and 10). The initial mixing ratio and potential temperature near the surface are 14.7 g kg^{-1} and 298.9 K, respectively. The sea surface temperature is assumed to be 302 K. Both simulations were performed for 3 h.

3. Results

The top row in Fig. 6 shows the fields of vertical velocities in the LE control run at time instances of 60, 130, and 180 min. It can be seen that the changes of the vertical velocity with height indicate the existence of large eddies, namely a relatively narrow regions of updrafts and downdraft with vertical scales of the computational

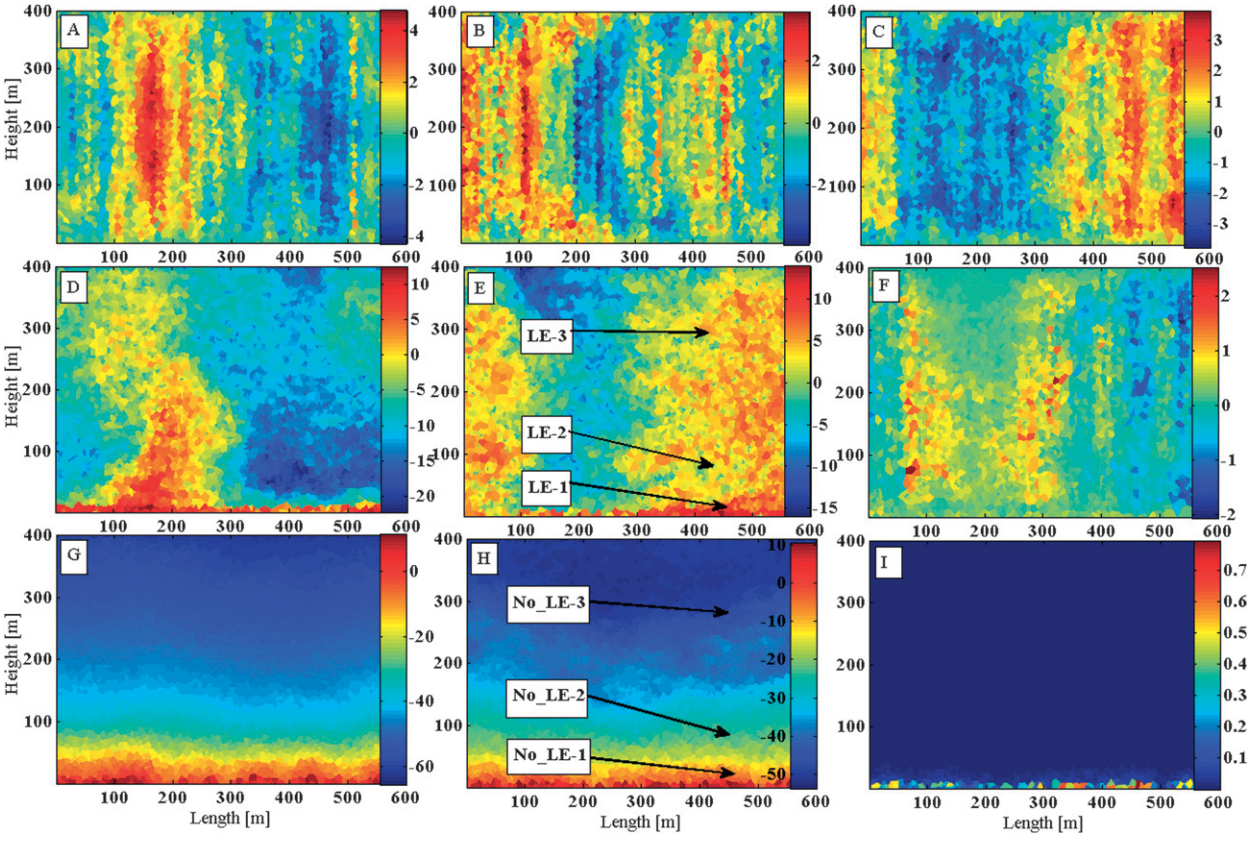

FIG. 6. (a)–(c) Fields of vertical velocity (m s^{-1}) at t = (a) 60, (b) 130, and (c) 180 min. (d)–(i) Radar reflectivity (dBZ) at t = (d),(g) 60 and (e),(h) 180 min, and (f),(i) the rain flux field (mm h^{-1}) at 180 min in the (d)–(f) LE and (g)–(i) No_LE simulations. Arrows in (e) and (h) show the parcels whose size distributions are presented in Fig. 7.

area depth. The maximum updraft velocities vary from about 1 to about 4 m s^{-1}. The middle row in Fig. 6 shows the LE run radar reflectivity fields at t = 60 and t = 130 min, as well as the rain flux at t = 180 min. Since the radar reflectivity is proportional to the sixth power of the droplet radius, higher values of radar reflectivity indicate the presence of larger droplets. In particular, high values of radar reflectivity within the lowest approximately 10-m layer point out at the presence of large droplets in the vicinity of a sea spray source. It can be seen that in the LE run, LE effectively transport spray upward. In Fig. 6 the fields shown in the bottom row belong to the No_LE run at the same simulation time of those in the middle row. While Fig. 6d illustrates the initial stage of spray penetrating into upper levels on top of updrafts (cf. Fig. 6a), Fig. 6e illustrates the advanced simulation stage where spray droplets form a ''spray-made'' cloud in both updrafts and downdrafts (cf Fig. 6b). Figure 6f shows the advanced simulation stage of spray evolution when drizzle droplets fall within the areas of downdrafts (see Fig. 6c for updraft/downdraft areas). It can be seen that the BL microphysical structure in the No_LE run (bottom) dramatically differs from that in the LE run. The sea spray ascending as a result of turbulent diffusion creates a stratified structure seen by a rapid decrease in the radar reflectivity with height, indicating a decrease both in the concentration and the size of large spray droplets. Figure 7 shows DSDs and the corresponding dry aerosol size distributions (aerosols within droplets) in specific parcels marked by arrows in the middle column of Fig. 6 at t = 130 min (Figs. 7e,h). These parcels were chosen randomly to illustrate the effect of DSD changes over height in the two runs. A dramatic difference can be seen in the manner DSD changes over height in the No_LE and LE runs. While the maximum droplet size at 300 m in the No_LE run is about 30 μm, it exceeds 200 μm in the LE run. The dry aerosol radius in both the LE and the No_LE runs indicates less dramatic changes. Nevertheless, the spectra show that even large spray droplets (with dry APs with radii of about 25 μm) reach levels of a few hundred meters while ascending in updrafts caused by large eddies. At the same time, in the No_LE run no drizzle form aloft and no rain flux is observed (Fig. 7i). The difference in the BL

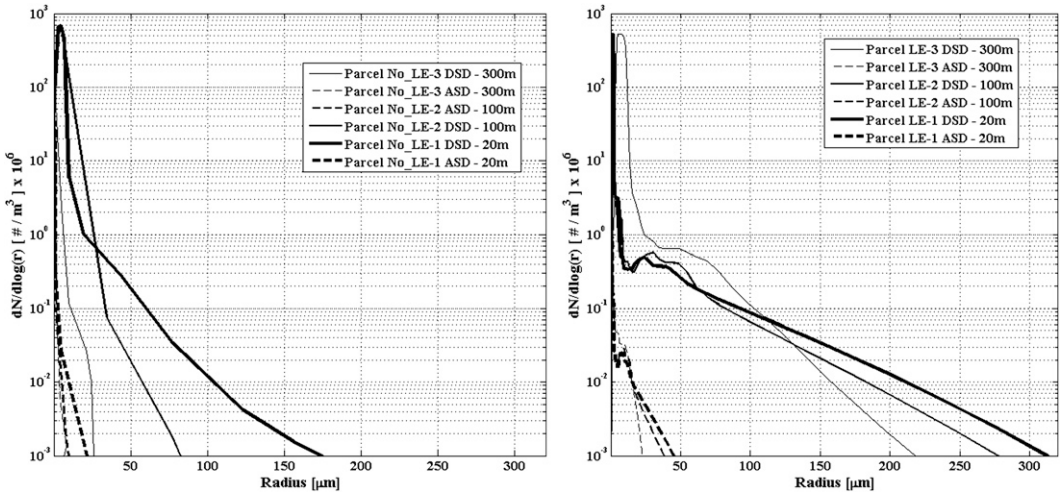

FIG. 7. DSDs and aerosol size distributions (ASDs) at different heights in the (left) No_LE and (right) LE simulations in parcels denoted by arrows in Fig. 6.

microphysical structure in the No_LE and LE runs is further illustrated in Fig. 8 showing the radar reflectivity–liquid water content (LWC) scatter diagram for both simulations. Each point in this diagram denotes a separate Lagrangian parcel. The height of the location of each air parcel is marked by the color of the corresponding point. In the No_LE run, within the lowest 50-m layer, the LWC and radar reflectivity maximum reach 0.4 g m^{-3} and 10 dBZ, respectively. The radar reflectivity and LWC rapidly decrease with increasing height, so at z = 150 m these quantities reduce to 0.1 g m^{-3} and −30 dBZ, respectively. Above about 150 m, LWC and radar reflectivity lower than 0.1 g m^{-3} and −30 dBZ, respectively, are accounted for by haze particles produced by the background APs. In the LE run, the scatter diagram is remarkably different from that in the No_LE run. In the LE run, parcels in the surface vicinity have a lower average LWC (~0.1 g m^{-3}) and a lower radar reflectivity (~5 dBZ) as compared to the No_LE run. This effect can be attributed to the transport of spray upward by LE. In contrast to the No_LE run, LWC in the LE run increases with height, which can be attributed to condensational growth of spray at high relative humidity. In spite of the fact that LWC increases with height, the radar reflectivity decreases with increasing height. We attribute this result to the sedimentation of largest droplets containing a comparatively low fraction of liquid mass but contributing significantly to the reflectivity.

Nonlocal vertical MBL mixing caused by parcel movement in the presence of LE leads to very different vertical profiles of the horizontally averaged mixing ratio and potential temperature, as compared to those formed by small-scale turbulent diffusion (see Figs. 9 and 10, respectively). As mentioned above, the SST was chosen to be equal to 302 K. One can see that in both runs the sensible fluxes and moisture fluxes lead to a general heating and moistening of the BL, though in very different manners. The LE run demonstrates formation of a well-mixed BL with a slightly warming tendency in the upper levels, which in our case can be attributed to droplet condensation. The profiles of potential temperature and mixing ratio obtained in the LE run agree well both qualitatively and quantitatively with those observed by Zhang et al. (2009) in the BL of TCs under strong wind conditions. The observed profiles indicate the existence of a well-mixed 400-m layer with the potential temperature slightly growing and the mixing ratio slightly decreasing with increasing height. Note that such temperature and mixing ratio profiles are typical for the MBL under moderate winds as well (e.g., Stevens et al. 2003, 2005). At the same time, the No_LE simulation demonstrates a higher rate of heating and moistening at the lower levels and much lower rates at the upper levels. Rough evaluation of the turbulent diffusion front propagation speed (proportional to $\sqrt{kt}$, where k is the turbulent viscosity coefficient) shows that the obtained profiles in the No_LE simulation correspond to an effective turbulent diffusion coefficient of about 10–15 m^2 s^{-1}. This value agrees well with turbulent diffusion coefficient estimation yielded by the similarity theory, corresponding to dissipation rate of about 220 cm^2 s^{-3}.

The differences in the vertical temperature and humidity profiles in the No_LE and LE simulations lead to significant differences in the vertical profiles of supersaturation (relative humidity). These differences are illustrated in Fig. 11 showing the supersaturation

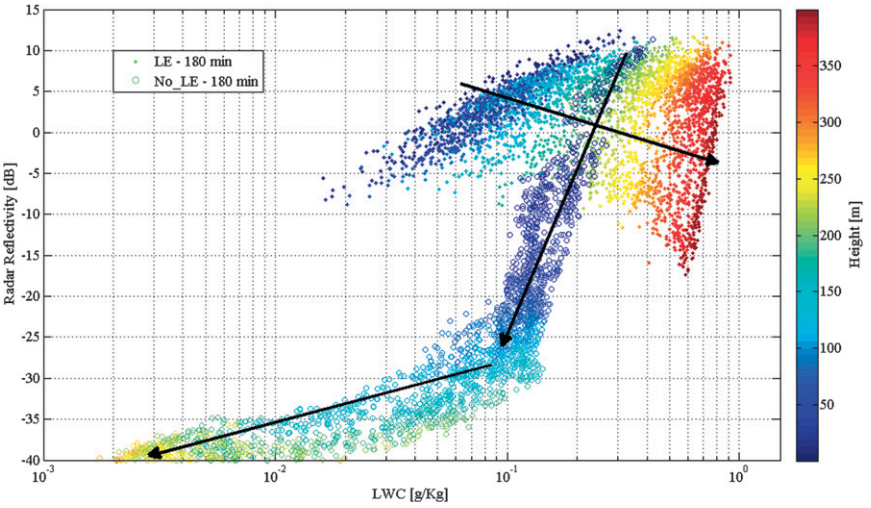

FIG. 8. Scatterplot diagram of radar reflectivity against LWC in the No_LE (open circles) and LE simulations (filled circles) at $t = 180$ min. Each scatter point corresponds to a separate air parcel. Arrows show the direction of the parcel ascent.

profiles during different time periods in the course of simulations. In the No_LE run, the relative humidity increases largely within the lower part of the BL; consequently toward $t \approx 120$ min it exceeds about 98% near the surface because of the intense surface moisture flux, which further leads to spray condensation in the vicinity of the spray source. At the same time, below 100–150 m the relative humidity in the LE run does not exceed 90%–95%, which, as will be shown below, leads to evaporation of spray.

In the LE run, the relative humidity increases largely at the upper levels because of humidity transport by LE. The latter leads to formation of a supersaturation layer near the upper boundary at $t = 90$ min. The depth of this layer increases with time and at $t = 180$ min its base is located at 200 m. The profiles of supersaturation indicate that in the LE run the evaporation within this layer is replaced by condensation. This tendency toward an increase in relative humidity due to vertical nonlocal mixing caused by LE is typical for formation of stratocumulus clouds

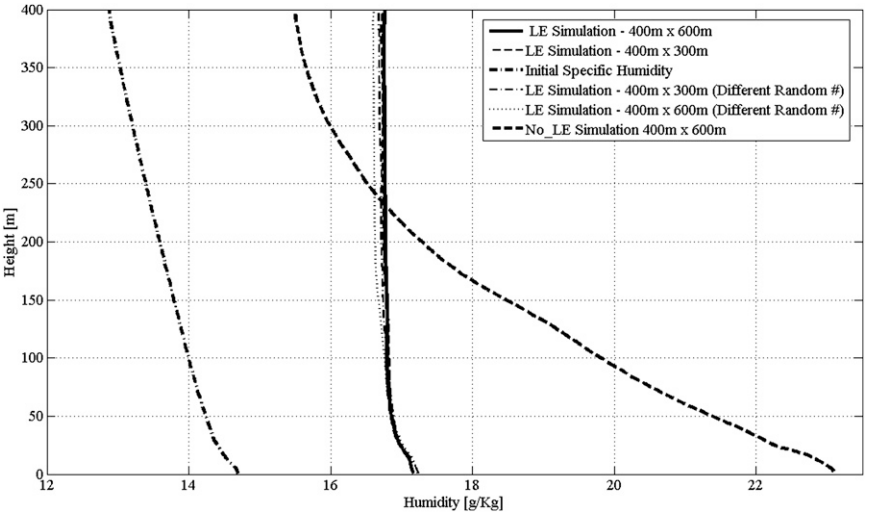

FIG. 9. Vertical profiles of horizontally averaged and simulation time–averaged mixing ratio in the No_LE (thick dashed) and LE simulations (thick solid). Profiles obtained in the LE simulations at other turbulence velocity field realizations, as well as at 300-m computational length, are shown by dashed, dashed–dotted, and dotted lines. The initial mixing ratio profile is shown by a thick dashed–dotted curve.

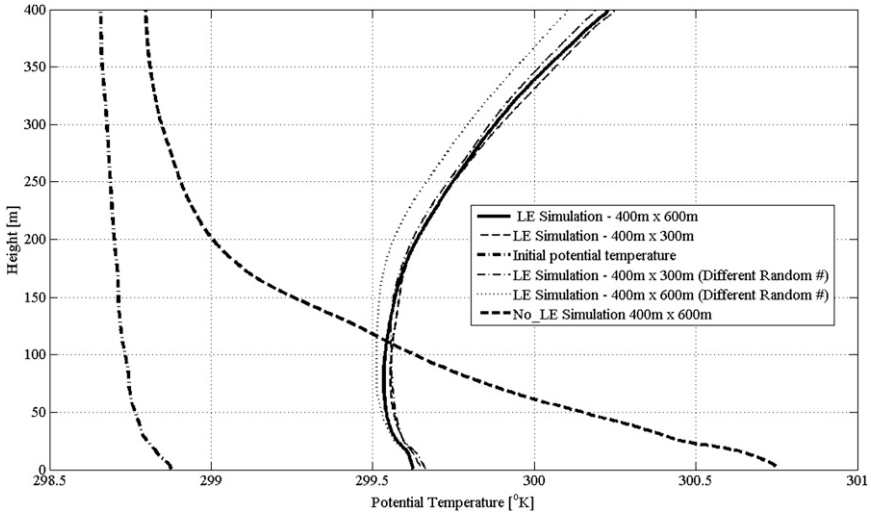

FIG. 10. Vertical profiles of horizontally averaged and simulation time–averaged potential temperature in the No_LE (thick dashed) and LE simulations (thick solid). Other line types are as in Fig. 9. The initial potential temperature profile is denoted by a thick dashed–dotted curve.

(Pinsky et al. 2008; Magaritz et al. 2009). The sea spray thermodynamic effects are largely determined by vertical mixing of humidity and droplet salinity caused by LE. Figure 12 shows the fields of salinity averaged over the droplet size distributions at $t = 10$ and $t = 180$ min. It can be seen that the salinity in the No_LE run (top row) is quite homogeneous in the horizontal direction and increases with height. The increase in salinity is caused by droplet evaporation, as a decrease in the amount of water in droplets is not accompanied by

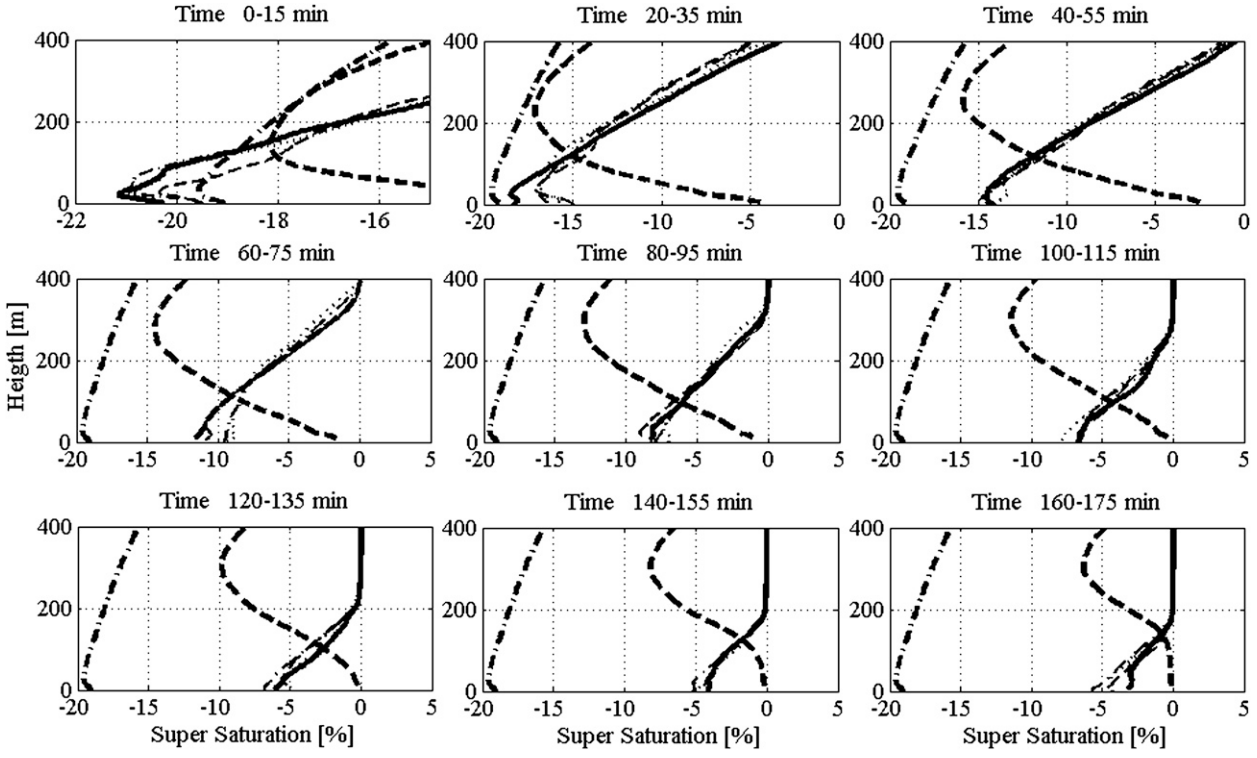

FIG. 11. Vertical profiles of supersaturation with simulation time in the LE (thick solid) and No_LE (thick dashed) simulations. Other line types are as in Fig. 9. Initial supersaturation is marked with a bold dashed–dotted curve.

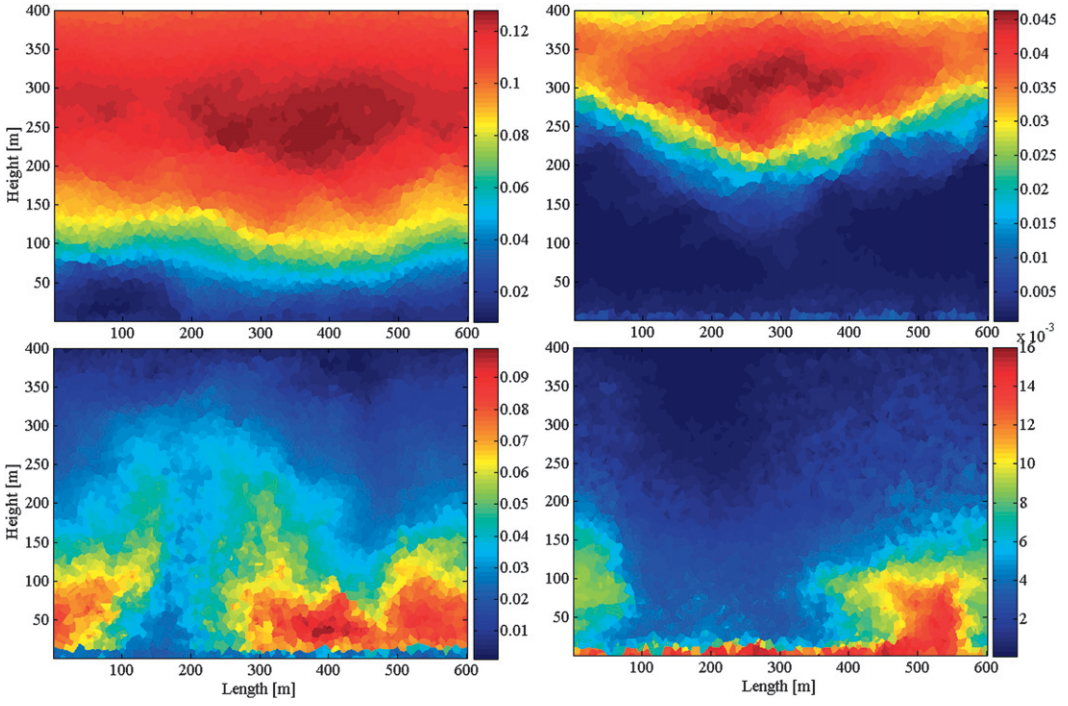

FIG. 12. Fields of droplet salinity in the (top) No_LE and (bottom) LE runs at (left) 10 and (right) 180 min. Note that the scales of the figures are of the same order but different in value.

a decrease in droplet salt content. In the LE run (bottom row), the general tendency of salinity variations is opposite to that in the No_LE run. In the LE run, larger values of salinity are associated mainly with the lower layer, just above the spray source location. At early simulation times the salinity has a maximum around 125 m, while later the salinity decreases with height increasing above about 50 m. This decrease in salinity with height can be attributed to the spray condensational growth. This behavior of salinity corresponds well to the profiles of supersaturation shown in Fig. 11. To get a better understanding of the difference in behavior of salinity, as well as the difference in thermodynamic processes within the upper parts of the BL, we present Fig. 13, which shows the Kohler diagram for wet spray particles of different radii. The figure presents two curves corresponding to the two values of salinity, namely 35 and 70 g kg^{-1}. As was mentioned above, the salinity of newly produced spray droplets was assumed to be equal to that of seawater (i.e., 35 g kg^{-1}, or 0.035). The points where the curve with initial salinity of 0.035 cross the Kohler curves correspond to the initial location of spray droplets in the Kohler diagram. One can see a specific microphysical feature of spray droplets: at RH below about 98%, all newly produced spray droplets evaporate. A partial evaporation of spray leads to an increase in salinity, as one can see in the lower part of the LE run just above the spray source location (Fig. 12). If a droplet radius decreases due to evaporation by 25%, its salinity increases by factor of 2. Figure 13 shows that if the salinity is 70 g kg^{-1}, most spray droplets grow by condensation at RH $>$ 96%, with the exception of the smallest particles with sizes below a few microns.

This analysis reveals two distinct mechanisms that determine the difference in condensation/evaporation regimes between the LE and No_LE runs. In the LE run, nonlocal vertical mixing leads to an increase in RH values at the upper part of the BL to values at which most spray droplets start growing by condensation (in this regime a decrease in salinity takes place). Evaporation (largely partial evaporation) of spray within the lowest 100-m layer in the LE run leads to an increase in salinity. It is noteworthy that in the LE run large spray drops are transported upward and start growing because of condensation at low RH (~95%). At the same time, RH in the No_LE run remains less than about 95% above 150–200 m during the entire simulation. Moreover, in the No_LE run mostly small background aerosols and small spray droplets may reach the upper levels, so their evaporation continues despite the increase in salinity. As a result, all droplets evaporate despite the increase in salinity in the upper half of the BL in the No_LE run.

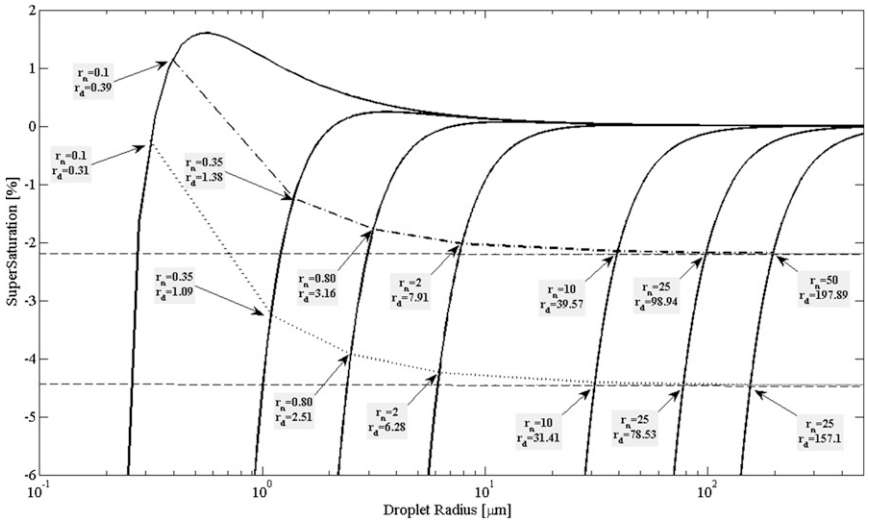

FIG. 13. Kohler equilibrium curves for NaCl (thick solid). The dashed–dotted curve denotes the relationship between dry and wet spray droplet size corresponding to the initial salinity assumed to be equal to that of ocean water (i.e., 35 g kg^{-1}). Notations: r_n is the dry aerosol radius (μm), and r_d corresponds to the equilibrium droplet radius size (μm). The dotted curve corresponds to salinity of 70 g kg^{-1}. According to the dashed–dotted curve, most micron/supermicron spray droplets are in equilibrium at supersaturation of $\sim -2\%$ (i.e., at RH $\approx$ 98%).

The differences in behavior of supersaturation determine the corresponding differences in the vertical profiles of the horizontally averaged LWC in the No_LE and LE runs (Fig. 14). It is noteworthy that the LWC near the surface is higher in the No_LE run, which can be attributed to a weaker vertical transport of large spray droplets in this run. Accordingly, the vertical gradient of spray loading just above the surface is higher in the No_LE run. In the No_LE run, the LWC rapidly decreases over height according to (or close enough to) the power law, in agreement with the results of 1D models. Such a high vertical gradient of LWC (i.e., loading gradient) within the lowest few tens of meters was the basis for all the theoretical studies considering the weakening of turbulence intensity and the drag coefficient as the reason leading to higher surface winds

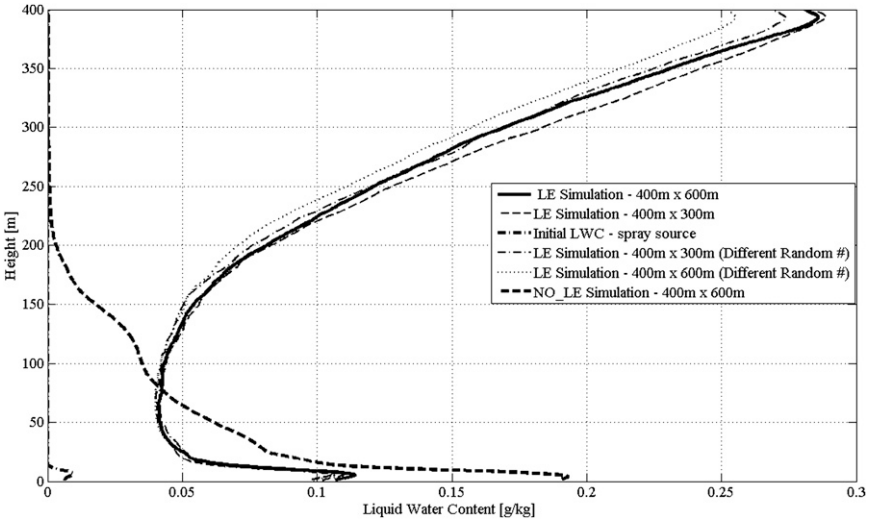

FIG. 14. Vertical profiles of horizontally averaged and simulation time–averaged LWC in the No_LE (thick dashed) and LE runs (thick solid). The LWC as a result of the spray source at t = 0 is marked by a dashed–dotted line. Other line types are as in Fig. 9.

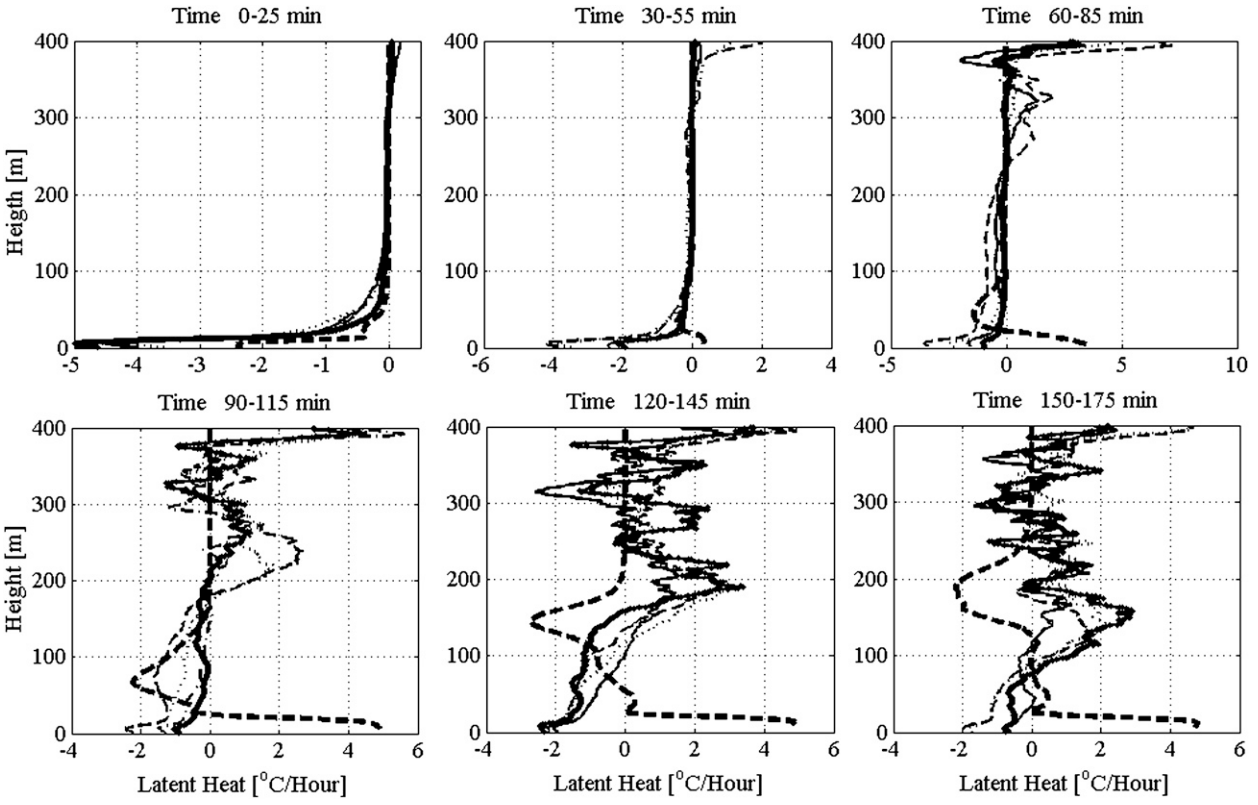

FIG. 15. Vertical profiles of horizontally averaged latent heat rate release at different time instances in the LE (thick solid) and No_LE runs (thick dashed). Other line types are as in Fig. 9.

(e.g., Kudryavtsev 2006). In the LE run, the vertical LWC profile can be separated into three main regions: (a) the lowest region at about 10–20 m characterized by a sharp decrease in LWC with height (this region forms as a result of the constant production of spray and rapid sedimentation of largest droplets); (b) the region of nearly constant LWC (~25–150 m) where there is a dynamic equilibrium between sedimentation and evaporation on the one hand and upward transport on the other; and (c) the upper layer where LWC increases by diffusion growth of spray and background APs in updrafts dominate over sedimentation. The increase in droplet size may also take place because of the collisions of spray droplets with other droplets and/or haze particles forming as a result of the background aerosols. This behavior of LWC agrees well with that seen in the radar reflectivity–LWC scatter diagram (Fig. 8). Comparison of LWC gradients in the No_LE and LE runs shows that large eddies significantly decrease the vertical loading gradient in the lowest tens of meters, making the mechanism of reducing turbulent intensity (and the drag coefficient) less efficient.

The values of supersaturation and LWC are closely related to the vertical profiles of the latent heat rate release across the MBL, determining the rate of air heating caused by condensation and air cooling caused by evaporation. Figure 15 shows the horizontally averaged rate of latent heat release at different time instances. At $t = 25$ min, the profiles in both simulations are quite similar, but the rates of cooling near the surface are different. The strong cooling in the LE run is caused by the continuously stronger evaporation of spray droplets within the region just above spray source height (the initial relative humidity was chosen to be equal to approximately 80% at the ground level as seen by the curve in Fig. 11). In the No_LE run, the area of cooling (and the increase in RH) propagates upward over time according to diffusion of relatively small spray droplets upward. No significant cooling or heating takes place above 250 m (at $t = 175$ min) since large enough spray droplets do not penetrate above this level. At the same time, the increase in humidity within the lowest 25-m layer, caused mostly by the moisture surface fluxes, leads to a gradual change from cooling caused by evaporation to heating caused by condensation, as discussed above.

In the LE run, undersaturation in the lower 100-m layer leads to cooling. In contrast, the increase in relative

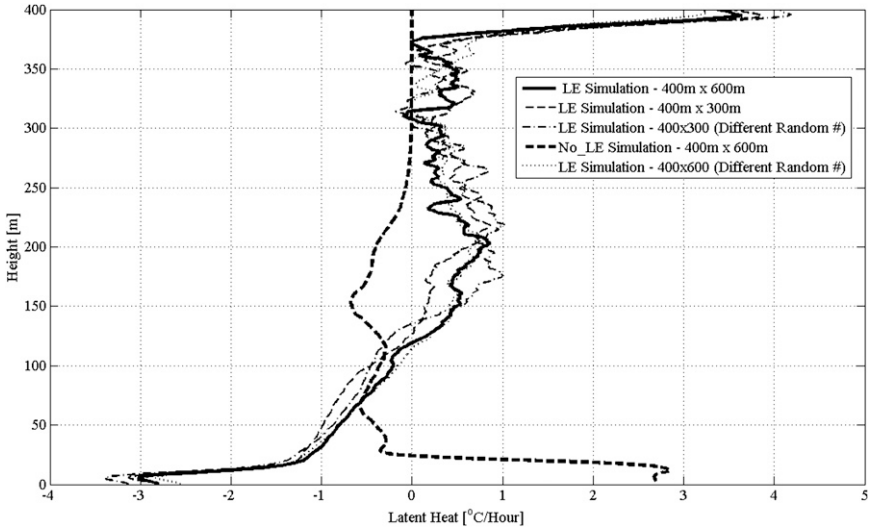

FIG. 16. Vertical profiles of horizontally averaged and simulation time–averaged latent heat rate release in the LE (thick solid) and No_LE runs (thick dashed). Other line types are as in Fig. 9.

humidity aloft leads to condensation and to subsequent heating. Cloud droplets arising near the upper boundary on background aerosols are the first to contribute to the heating process. At about 60 min, ''spray-formed'' cloud emerges at the upper boundary, and evaporative cooling forms because of large droplets' sedimentation. An increase in humidity by nonlocal mixing and by settling of spray droplets moves the boundary between heating (top layers) and cooling (bottom layers) downward. At $t = 150$ min, heating takes place within the whole BL layer above the 100-m level. Figure 16 summarizes the microphysical effects of spray in the presence/absence of LE. The figure shows vertical profiles of horizontally averaged and time averaged latent heat rate release in the LE and No_LE runs. It can be seen that LE combined with spray production can gradually change the sign of the microphysical effects across the entire BL as seen from the latent heat field.

The nonlocal mixing of the BL in the LE run causes a significant increase in the sensible and latent surface fluxes as compared with the No_LE simulation, as shown in Fig. 17. Initial high flux values are related to the

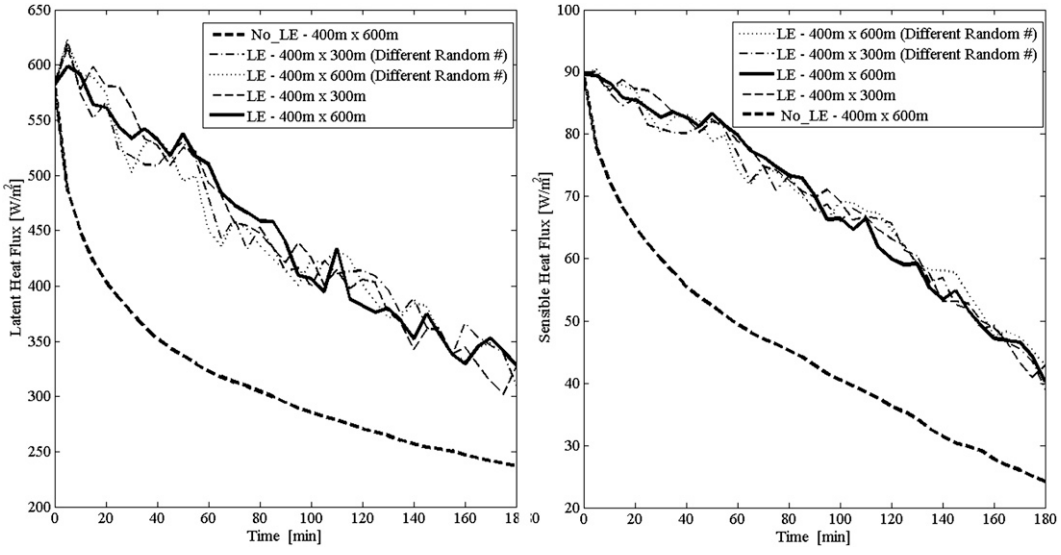

FIG. 17. Time dependence of (left) latent heat surface fluxes and (right) sensible heat surface fluxes in the LE (thick solid) and No_LE runs (thick dashed). Other line types are as in Fig. 9.

response to the initial relatively cold and dry atmosphere. The value of the latent heat surface flux in the LE run tends to about 330 W m^{-2}. This value agrees well with the result of measurements reported by Zhang et al. (2009) and substantially exceeds the values of flux calculated in the No_LE run (~230 W m^{-2}). One can see that the BL mixing caused by large eddies increases the surface fluxes by factors as high as 1.5–2. This evaluation agrees with the evaluation of the impact of large eddies on the surface moisture fluxes obtained in previous studies (e.g., Ginis et al. 2004).

The results of the sensitivity simulations with different turbulent velocity field realizations and for the 300-m-long computational area are shown in Figs. 9–11 and 14–16. One can see that the general structure of the BL is not sensitive either to different velocity realizations or to the computational area length, at least within the range used in this study. The intensity of large eddies is determined largely by the profile of $\langle w'^2 \rangle^{1/2}(z)$, which was similar in all the simulations. It is noteworthy that a quite low sensitivity of BL convective cells intensity to their aspect ratio was reported in a number of studies (e.g., Ivanov and Khain 1976b; Khain and Ingel 1995). This low sensitivity is one of the factors that make the problem of preferable aspect ratio of BL convective cells difficult to solve. Therefore, the results of our supplementary simulations justify the robustness of the results with regard to LE effects.

4. Conclusions

The structure of the MBL under conditions of moderate to strong winds, as well as surface sensible fluxes and latent heat fluxes, is determined largely by the combined effects of microphysical processes related to spray and the MBL dynamical properties. According to observations, the hurricane BL is characterized by the existence of large eddies often associated with convective cells. Based on the results of previous studies (e.g., Khain et al. 1986; Khain and Ingel 1988, 1995; Ginis et al. 2004; Zhang et al. 2008), we focused this study on the effects of large eddies on the thermodynamic structure of hurricane BL in the presence of wind-dependent sea spray production.

Spray production was included in a 2D Lagrangian boundary layer model with explicit spectral bin microphysics. The BL is covered by 3750 adjacent interacting Lagrangian parcels moving in a turbulent-like flow obeying the $-5/3$ Kolmogorov law. The turbulent-like flow contains harmonics within a wide range of scales including large eddies with scales of several hundred meters. The model calculates explicitly the diffusion growth/evaporation and collisions/sedimentation of droplets (both as sea spray droplets and as background aerosols), as well as aerosol masses within droplets. The turbulent mixing between the Lagrangian parcels playing the role of a small-scale turbulent diffusion of thermodynamic and microphysical variables was explicitly taken into account. Background aerosol particles serving as cloud condensation nuclei with size distributions typical of the maritime BL were included. The continuous generation of sea spray is determined by a spray source function obtained by matching ultramicron (>10 μm) and submicron distributions. The source function and the surface fluxes were calculated for a background wind speed of 20 m s^{-1}.

The results of the two simulations were compared. In the first simulation (the LE run), parcels were advected by a turbulent-like velocity field containing large vortices associated with large eddies. The rms of the vertical velocity fluctuations across the 400-m layer was assumed to be equal to 1.22 m s^{-1}, which agrees with observations for 20 m s^{-1} background wind. In the second simulation (the No_LE run), parcels were motionless, so vertical fluxes of humidity and temperature, as well as droplet size distribution, were caused by small-scale turbulent fluxes between adjacent parcels.

It has been shown that LE lead to formation of a well-mixed BL that agrees well with the observed structure of a TC boundary layer. LE substantially decreases the LWC gradient (i.e., the air density loading gradient) within the 50-m layer near the surface. This LE effect suggests that the mechanism of the buoyancy-driven decrease in turbulence intensity and in the drag coefficient is less universal than earlier suggested.

LE transports spray droplets and aerosols to high levels, causing substantially different vertical profiles of relative humidity and latent heat release as compared to the case when only turbulent diffusion mechanism is assumed. Strong updrafts related to LE in the BL transport a significant amount of large spray to the cloud-base level, thus accelerating rain formation in clouds, as well as producing drizzling clouds with a cloud base at about the 200-m height. The presence of spray makes the definition of cloud base at high wind speeds a challenging problem, as spray induces precipitation within the whole BL. It has been also further shown that LE are the main dynamic factor leading the simulation to observed sensible fluxes and latent heat surface fluxes. The surface fluxes in the presence of LE are by 50%–100% higher than in the case when the transport is determined by small-scale turbulence only. It has been shown that the results are practically insensitive to changes of the length of the computational area within the 300–600-m range.

Future studies are planned to investigate the effects of different background wind speeds (and the corresponding

spray production intensity) and sea surface temperature on the thermodynamics and microstructure of the BL as well as on the surface fluxes.

Acknowledgments. The authors express their deep gratitude to J. Zhang and C. Fairall for their interest in this study and for their valuable comments. The study was supported by the Israel Science Foundation (Grant 140/07) and by the Hurricane Aerosol Microphysics Project (HAMP).

REFERENCES

Andreae, M. O., and D. Rosenfeld, 2008: Aerosol–cloud–precipitation interactions. Part 1: The nature and sources of cloud-active aerosols. *Earth Sci. Rev.,* **89,** 13–41.

Andreas, E. L, 1995: The temperature of evaporating sea spray droplets. *J. Atmos. Sci.,* **52,** 852–862.

——, 1998: A new sea spray generation function for wind speed up to 32 m s^{-1}. *J. Phys. Oceanogr.,* **28,** 2175–2184.

Bao, J.-W., C. W. Fairall, and S. A. Michelson, 2007: The first semiannual report of the project entitled ''Evaluation and Improvement of Spray-Modified Air–Sea Enthalpy and Momentum Flux Parameterizations for Operational Hurricane Prediction.'' Tropical Prediction Center, 23 pp.

——, ——, and ——, 2009: The final report of the project entitled ''Evaluation and Improvement of Spray-Modified Air–Sea Enthalpy and Momentum Flux Parameterizations for Operational Hurricane Prediction.'' Tropical Prediction Center, 34 pp. [Available online at http://origin.www.nhc.noaa.gov/jht/07-09reports/final_Bao_JHT09.pdf.]

Bott, A., 1989: A positive definite advection scheme obtained by nonlinear renormalization of the advective fluxes. *Mon. Wea. Rev.,* **117,** 1006–1015.

Bryan, K., 1966: A scheme for numerical integration of the equations of motion on an irregular grid free of nonlinear instability. *Mon. Wea. Rev.,* **94,** 39–40.

Clarke, A. D., S. R. Owens, and J. C. Zhou, 2006: An ultrafine sea-salt flux from breaking waves: Implications for cloud condensation nuclei in the remote marine atmosphere. *J. Geophys. Res.,* **111,** D06202, doi:10.1029/2005JD006565.

Davidson, K. L., and L. Schutz, 1983: Observational results on the influence of surface layer stability and inversion entrainment on surface layer marine aerosol number density. *Opt. Eng.,* **22,** 45–49.

Drennan, W. M., J. A. Zhang, J. R. French, C. McCormick, and P. G. Black, 2007: Turbulent fluxes in the hurricane boundary layer. Part II: Latent heat flux. *J. Atmos. Sci.,* **64,** 1103–1115.

Edson, J. B., and C. W. Fairall, 1994: Spray droplet modeling. 1. Lagrangian model simulation of the turbulent transport of evaporating droplets. *J. Geophys. Res.,* **99,** 25 295–25 311.

——, S. Anquetin, P. G. Mestayer, and J. F. Sini, 1996: Spray droplet modeling. 2. An interactive Eulerian–Lagrangian model of evaporating spray droplets. *J. Geophys. Res.,* **101,** 1279–1293.

Fairall, C. W., J. B. Edson, and M. A. Miller, 1990: Heat fluxes, whitecaps, and sea spray. *Surface Waves and Fluxes,* Vol. 1, G. L. Geernaert and W. J. Plant, Eds., Kluwer, 173–208.

——, J. D. Kepert, and G. J. Holland, 1994: The effect of sea spray on surface energy transports over the ocean. *Global Atmos. Ocean Syst.,* **2,** 121–142.

——, M. L. Banner, W. L. Peirson, W. Asher, and R. P. Morison, 2009: Investigation of the physical scaling of sea spray spume droplet production. *J. Geophys. Res.,* **114,** C10001, doi:10.1029/2008JC004918.

Foster, R. C., 2005: Why rolls are prevalent in the hurricane boundary layer. *J. Atmos. Sci.,* **62,** 2647–2661.

French, J. R., W. M. Drennan, J. A. Zhang, and P. G. Black, 2007: Turbulent fluxes in the hurricane boundary layer. Part I: Momentum flux. *J. Atmos. Sci.,* **64,** 1089–1102.

Garratt, J. R., 1994: *The Atmospheric Boundary Layer*. Cambridge University Press, 316 pp.

Ginis, I., A. Khain, and E. Morozovsky, 2004: Effects of large eddies on the structure of the marine boundary layer under strong wind conditions. *J. Atmos. Sci.,* **61,** 3049–3063.

Gong, S. L., 2003: A parameterization of sea-salt aerosol source function for sub- and super-micron particles. *Global Biogeochem. Cycles,* **17,** 1097, doi:10.1029/2003GB002079.

Ingel, L. Kh., 2011: Effects of spray on dynamics of surface layer under strong winds. *Atmos. Oceanic Phys.,* **47,** 1–9.

Ivanov, V. N., and A. P. Khain, 1975: On dry and moist cellular convection in the atmosphere. *Atmos. Oceanic Phys.,* **11,** 1211–1219.

——, and ——, 1976a: On characteristic values of Rayleigh numbers during the development of cellular convection in turbulent atmosphere. *Atmos. Oceanic Phys.,* **12,** 23–28.

——, and ——, 1976b: On the maximum principle and the preferable wave number in dry and moist cellular convection. *Atmos. Oceanic Phys.,* **12,** 325.

Kepert, J., C. W. Fairall, and J. W. Bao, 1999: Modelling the interaction between the atmospheric boundary layer and evaporating sea spray droplets. *Air–Sea Exchange: Physics, Chemistry, and Dynamics,* G. L. Geernaert, Ed., Kluwer Academic, 363–409.

Khain, A. P., and L. Kh. Ingel, 1988: A numerical model of the atmospheric boundary layer above the ocean in the presence of convection. *Atmos. Oceanic Phys.,* **24,** 24–32.

——, and ——, 1995: Numerical modeling of interaction of a non-stationary divergent flow with convective processes in the boundary layer over the ocean. *Atmos. Oceanic Phys.,* **31,** 496–506.

——, M. G. Yarmolinskaya, and L. Kh. Ingel, 1986: Numerical modeling of interaction of convective and large-scale processes in the atmospheric boundary layer with the formation of a temperature inversion. *Atmos. Oceanic Phys.,* **22,** 987–993.

——, M. Pinsky, L. Magariz, O. Krasnov, and H. W. J. Russchenberg, 2008: Combined observational and model investigations of the *Z*–LWC relationship in stratocumulus clouds. *J. Appl. Meteor. Climatol.,* **47,** 591–606.

Kudryavtsev, V. N., 2006: On the effect of sea drops on the atmospheric boundary layer. *J. Geophys. Res.,* **111,** C07020, doi:10.1029/2005JC002970.

LeMone, M. A., 1973: The structure and dynamics of horizontal roll vortices in the planetary boundary layer. *J. Atmos. Sci.,* **30,** 1077–1091.

Lenschow, D. H., J. C. Wyngaard, and W. T. Pennell, 1980: Mean-field and second-moment budgets in a baroclinic, convective boundary layer. *J. Atmos. Sci.,* **37,** 1313–1326.

Lewis, E. R., and S. E. Schwartz, 2004: *Sea Salt Aerosol Production: Mechanisms, Methods, Measurements and Models—A Critical Review*. *Geophys. Monogr.,* Vol. 152, Amer. Geophys. Union, 413 pp.

Lorsolo, S., J. L. Schroender, P. Dodge, and F. Marks, 2008: An observational study of hurricane boundary layer small-scale coherent structures. *Mon. Wea. Rev.,* **136,** 2871–2893.

Lothon, M., D. H. Lenschow, D. Leon, and G. Vali, 2005: Turbulence measurements in marine stratocumulus with airborne Doppler radar. *Quart. J. Roy. Meteor. Soc.,* **131,** 2063–2080.

Magaritz, L., M. Pinsky, O. Krasnov, and A. Khain, 2009: Investigation of droplet size distributions and drizzle formation using a new trajectory ensemble model. Part II: Lucky parcels in non-mixing limit. *J. Atmos. Sci.,* **66,** 781–805.

Makin, V. K., 1998: Air–sea exchange of heat in the presence of wind waves and spray. *J. Geophys. Res.,* **103,** 1137–1152.

——, 2005: A note on drag of the sea surface at hurricane winds. *Bound.-Layer Meteor.,* **115,** 169–176.

Mårtensson, E. M., E. D. Nilsson, G. de Leeuw, L. H. Cohen, and H. C. Hansson, 2003: Laboratory simulations and parameterization of the primary marine aerosol production. *J. Geophys. Res.,* **108,** 4297, doi:10.1029/2002JD002263.

Mestayer, P. G., A. M. J. Van Eijk, G. De Leeuw, and B. Tranchant, 1996: Numerical simulation of the dynamics of sea spray over the waves. *J. Geophys. Res.,* **101,** 20 771–20 797.

Monahan, E. C., D. E. Spiel, and K. L. Davidson, 1986: A model of marine aerosol generation via whitecaps and wave disruption. *Oceanic Whitecaps and Their Role in Air–Sea Exchange Processes,* E. C. Monahan and G. MacNiocaill, Eds., Reidel, 167–174.

Mueller, J. A., and F. Veron, 2009: A Lagrangian stochastic model for heavy particle dispersion in the atmospheric marine boundary layer. *Bound.-Layer Meteor.,* **130,** 229–247.

O'Dowd, C. D., and G. de Leeuw, 2007: Marine aerosol production: A review of the current knowledge. *Philos. Trans. Roy. Soc.,* **365A,** 1753–1774.

Pinsky, M., and A. P. Khain, 2002: Effects of in-cloud nucleation and turbulence on droplet spectrum formation in cumulus clouds. *Quart. J. Roy. Meteor. Soc.,* **128,** 501–533.

——, ——, and M. Shapiro, 2001: Collision efficiency of drops in a wide range of Reynolds numbers: Effects of pressure on spectrum evolution. *J. Atmos. Sci.,* **58,** 742–764.

——, L. Magaritz, A. P. Khain, O. Krasnov, and A. Sterkin, 2008: Investigation of droplet size distributions and drizzle formation using a new trajectory ensemble model. Part I: Model description and first results in nonmixing limit. *J. Atmos. Sci.,* **65,** 2064–2086.

——, A. P. Khain, and L. Magaritz, 2010a: Representing turbulent mixing of non-conservative values in Eulerian and Lagrangian cloud models. *Quart. J. Roy. Meteor. Soc.,* **136,** 1228–1242.

——, O. Krasnov, J. H. W. Russchenberg, and A. Khain, 2010b: Investigation of the turbulent structure of a cloud-capped mixed layer using Doppler radar. *J. Appl. Meteor. Climatol.,* **49,** 1170–1190.

Powell, M., P. Vickery, and T. Reinhold, 2003: Reduced drag coefficient for high wind speeds in tropical cyclones. *Nature,* **422,** 279–283.

Rosenfeld, D., R. Lahav, A. Khain, and M. Pinsky, 2002: The role of sea spray in cleansing air pollution over ocean via cloud processes. *Science,* **297,** 1667–1670.

Rouault, M. P., P. G. Mestayer, and R. Schiestel, 1991: A model of evaporating spray droplet dispersion. *J. Geophys. Res.,* **96,** 7181–7200.

Stevens, B., W. R. Cotton, and G. Feingold, 1998: A critique of one- and two-dimensional models of boundary layer clouds with binned representations of droplet microphysics. *Atmos. Res.,* **47-48,** 529–553.

——, C. H. Moeng, and P. P. Sullivan, 1999: Large-eddy simulations of radiatively driven convection: Sensitivities to the representation of small scales. *J. Atmos. Sci.,* **56,** 3963–3984.

——, and Coauthors, 2003: Dynamics and Chemistry of Maritime Stratocumulus: DYCOMS-II. *Bull. Amer. Meteor. Soc.,* **84,** 579–593.

——, and Coauthors, 2005: Evaluation of large-eddy simulations via observations of nocturnal marine stratocumulus. *Mon. Wea. Rev.,* **133,** 1443–1462.

Stull, R. B., 1988: *An Introduction to Boundary Layer Meteorology*. Kluwer Academic, 647 pp.

Toba, Y., 1965: On the giant sea-salt particles in the atmosphere. II: Theory of the vertical distribution in the 10-m layer over the ocean. *Tellus,* **17,** 365–382.

Van Eijk, A. M. J., B. S. Tranchant, and P. G. Mestayer, 2001: SeaCluse: Numerical simulations of evaporating sea spray droplets. *J. Geophys. Res.,* **106,** 2573–2588.

Van Zanten, M. C., B. Stevens, G. Vali, and D. H. Lenschow, 2005: Observations of drizzle in nocturnal marine stratocumulus. *J. Atmos. Sci.,* **62,** 88–106.

Xue, H., and G. Feingold, 2006: Large-eddy simulations of trade wind cumuli: Investigation of aerosol indirect effects. *J. Atmos. Sci.,* **63,** 1605–1622.

Zhang, J. A., 2010: Estimation of dissipative heating using low-level in situ aircraft observations in the hurricane boundary layer. *J. Atmos. Sci.,* **67,** 1853–1862.

——, K. B. Katsaros, P. G. Black, S. Lehner, J. R. French, and W. M. Drennan, 2008: Effects of roll vortices on turbulent fluxes in the hurricane boundary layer. *Bound.-Layer Meteor.,* **128,** 173–189, doi:10.1007/s10546-008-9281-2.

——, W. M. Drennan, P. G. Black, and J. R. French, 2009: Turbulent structure of the hurricane boundary layer between the outer rainbands. *J. Atmos. Sci.,* **66,** 2455–2467.